

Quantum magnetic oscillations in the absence of closed electron trajectories

Z. E. Krix,^{1,2,*} O. A. Tkachenko,³ V. A. Tkachenko,^{3,4} D. Q. Wang,^{1,2} O. Klochan,^{1,2} A. R. Hamilton,^{1,2} and O. P. Sushkov^{1,2}

¹*School of Physics, The University of New South Wales, Sydney, 2052, Australia*

²*Australian Research Council Centre of Excellence in Low-Energy Electronics Technologies, The University of New South Wales, Sydney 2052, Australia*

³*Rzhanov Institute of Semiconductor Physics, Novosibirsk, 630090, Russia*

⁴*Novosibirsk State University, Novosibirsk, 630090, Russia*

(Dated: April 9, 2024)

Quantum magnetic oscillations in crystals are typically understood in terms of Bohr-Sommerfeld quantisation, the frequency of oscillation is given by the area of a closed electron trajectory. However, since the 1970s, oscillations have been observed with frequencies that do not correspond to closed electron trajectories and this effect has remained not fully understood. Previous theory has focused on explaining the effect using various kinetic mechanisms, however, frequencies without a closed electron orbit have been observed in equilibrium and so a kinetic mechanism cannot be the entire story. In this work we develop a theory which explains these frequencies in equilibrium and can thus be used to understand measurements of both Shubnikov-de Haas and de Haas-van Alphen oscillations. We show, analytically, that these frequencies arise due to multi-electron correlations. We then extend our theory to explain a recent experiment on artificial crystals in GaAs two-dimensional electron gases, which revealed for the first time magnetic oscillations having frequencies that are half of those previously observed. We show that the half-frequencies arise in equilibrium from single-particle dynamics with account of impurities. Our analytic results are reinforced by exact numerics, which we also use to clarify prior works on the kinetic regime.

I. INTRODUCTION

Quantum oscillations in a magnetic field have a long history; both the Shubnikov-de Haas and de Haas-van Alphen effects belong to textbooks [1]. In these effects the resistance or the magnetisation are periodic functions of inverse magnetic field with “frequency” equal to the area of the Fermi surface. Quantum magnetic oscillations become slightly more complex in the magnetic breakdown regime, where tunneling between different Fermi surfaces is possible and results in multiple additional frequencies. This regime was discovered in quantum oscillations in magnesium [2] and was studied in numerous experiments after. Quantum magnetic oscillations are an important experimental tool for the study of solids, in part because of their relation to the size of the Fermi surface. They are used in topological materials [3, 4], in cuprates [5, 6] in twisted bilayer graphene [7] and in many other systems. In spite of the very long history of studies, one type of quantum magnetic oscillations, the type that we call “non-Onsager” throughout this work, has not been fully understood theoretically. Moreover, recent experiments on two-dimensional artificial crystals built on a GaAs two-dimensional electron gas (2DEG) have discovered a new type of magnetic oscillation effect: half-frequency non-Onsager oscillations [8]. The goal of the present work is to explain the non-Onsager effects and to develop a theory which accounts for both their frequency and the temperature dependence of their amplitude.

Standard quantum magnetic oscillations are described well by Onsager’s semi-classical picture [9]: an electron in a magnetic field undergoes periodic motion, orbiting along the Fermi surface (see Fig. 1a). Quantum oscillations of resistivity and magnetisation arise due to Bohr-Sommerfeld quantization of this motion. The oscillations are periodic in inverse magnetic field and the oscillation frequency is proportional to the cross-sectional area of the Fermi surface, which we denote by A_0 for a circular Fermi surface.

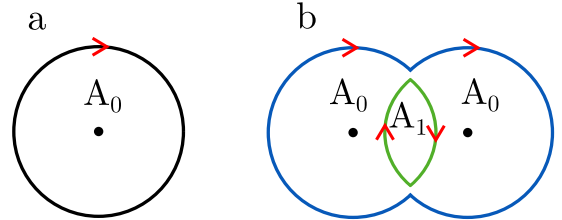


Figure 1. Panel a: simple Fermi surface and the corresponding circular trajectory in magnetic field. The corresponding frequency of quantum oscillations is A_0 , the area of the Fermi surface. Panel b: additional closed semiclassical trajectories that arise due to quantum jumps induced by Bragg scattering from the periodic potential. The corresponding frequencies of quantum oscillations are A_1 , $2A_0 - A_1$, $A_0 + A_1$.

When an electron gas is submerged in a periodic potential, magnetic breakdown can arise in addition to simple Bohr-Sommerfeld quantization. The potential can have a chemical origin, such as the lattice of a crystal, or it can have an artificial origin, such as an external modulation in a 2DEG [10]. Magnetic breakdown is a quantum correction to the simple Onsager picture, and was dis-

* z.krix@unsw.edu.au

covered in magnesium in the 1960s [2]. The origin of the effect is illustrated in panel b of Fig.1. Two electron orbits (blue circles) arise due to diffraction on the periodic potential. When the orbits intersect there is a probability that an electron will quantum mechanically jump from one circle to another. Hence, in addition to A_0 , quantum oscillations manifest A_1 , $2A_0 - A_1$, and $A_0 + A_1$ frequencies, where A_1 is the “elliptical” orbit drawn in green. In essence this is the same Onsager picture, only the number of possible trajectories is increased due to quantum jumps. Therefore, we call all these oscillations (frequencies) Onsager quantum oscillations. This is the magnetic breakdown regime. It is worth noting that the notion of Fermi surface is somewhat ambiguous in this regime. Multiple Onsager quantum oscillations have been observed in numerous experiments.

The multiple Onsager quantum oscillations are not puzzling, what is puzzling is that magnetic oscillations with frequency $A_0 - A_1$ have also been observed! Of course, the moon-shaped “trajectory” with area $A_0 - A_1$ exists in Fig. 1b. However, an electron cannot traverse along this “trajectory” since in a magnetic field the electron must travel in the same direction along each circular arc. The $A_0 - A_1$ oscillations are beyond the Onsager picture; we refer to them as non-Onsager oscillations. Non-Onsager oscillations can be more complex than just $A_0 - A_1$, however, they share the same property of not being traversable by an electron. Below, we enumerate some observations relating to these kinds of oscillations.

(i) Non-Onsager oscillations $A_0 - A_1$ have been observed in transport experiments, first in Magnesium [11, 12], then in laterally modulated, GaAs 2DEGs [13, 14], and later in organic metals [15, 16]. A common feature is that they decay with temperature much more slowly than Onsager oscillations. In semiconductors these oscillations are called Weiss oscillations or “commensurate oscillations”.

(ii) In the limit of very large wavelength of the external potential the “commensurate oscillations” in transport have been explained on the basis of the single particle kinetic equation as an essentially non-equilibrium effect [12, 17–19]. The theoretical work Ref.[20] explicitly claims that non-Onsager oscillations can appear only in resistivity and not in magnetisation. In a sense, the single particle non-equilibrium kinetic equation mechanism implies that “commensurate oscillations” are magnetic oscillations, but they are not quantum magnetic oscillations.

(iii) Contrary to the single electron kinetic mechanism, non-Onsager magnetic oscillations have been also observed in magnetisation measurements in magnesium [21] and in organic metals [16]. This means the effect exists in equilibrium as well. It does not mean that the non-equilibrium kinetic equation mechanism [12, 17–19] is wrong, however, it does mean that kinetics is only a part of the story.

(iv) There is another twist related to 2D organic metals. It is well known that with variations of the magnetic

field in 2D gated systems the electron density is constant while the chemical potential is oscillating. There is a claim in literature [22] that non-Onsager quantum oscillations arise as combinatorial frequencies between the chemical potential oscillations and oscillations in the grand potential, so non-Onsager frequencies cannot exist at constant chemical potential. However, it has been pointed out later [23] that the “oscillating chemical potential” explanation cannot be correct since non-Onsager frequencies have also been observed in magnesium at constant chemical potential. Moreover, the observed non-Onsager quantum oscillations decay with temperature very slow, slower than the main oscillations A_0 . At the same time the mechanism related to oscillations of the chemical potential results in extremely fast decay with temperature.

To summarise points (i)-(iv), there is no consistent understanding of the mechanism of the non-Onsager magnetic oscillations. In our recent transport experiment [8] on a triangular lattice of anti-dots in a GaAs 2DEG we observed the non-Onsager oscillations $A_0 - A_1$ as well as other non-Onsager and Onsager oscillations that have not been previously observed. Moreover, we have also discovered half-frequency non-Onsager and Onsager oscillations with frequencies such as $(A_0 - A_1)/2$ and $(A_0 + A_1)/2$. Half-frequency oscillations have not been observed in any previous experiments and have not been discussed in any previous theoretical works. The important observation that sheds light on the mechanism is that amplitudes of $A_0 - A_1$ and $(A_0 - A_1)/2$ oscillations decay with temperature much slower than the amplitudes of Onsager oscillations.

The purpose of this paper is to explain these non-Onsager quantum oscillations. First, we resolve the controversy of “known” non-Onsager oscillations (“known” meaning prior to Ref. [8]). We demonstrate that there are two mechanisms: (i) single particle kinetics, and (ii) multi-electron correlations due to the Coulomb electron-electron interaction. Both mechanisms contribute to the Shubnikov–de Haas effect (transport) and only the second mechanism contributes to the de Haas–Van Alphen effect (equilibrium). We calculate the temperature dependence of quantum non-Onsager oscillations and hence explain why they survive up to relatively high temperatures in spite of being fully quantum. Second, we explain the recently discovered half-frequencies [8]. Here there are also two mechanisms, both single particle: (i) single particle kinetics, (ii) single particle dynamics with account of impurities. Both mechanisms contribute to the Shubnikov–de Haas effect (transport) and only the second mechanism contributes to the De Haas–Van Alphen effect (equilibrium). The mechanism (ii) conceptually has a distant similarity to the Al’tshuler-Aronov-Spivak effect [24].

The structure of the paper is the following. In section II we find analytically energies and wave functions of an electron in superimposed 1D periodic potential and magnetic field. The main conclusion is that the density

of states (DOS) does not contain non-Onsager frequencies. In Section III we solve numerically the problem of electron transport through a region with modulated potential. We consider a 1D periodic potential and a 2D triangular lattice. The numerical approach confirms that non-Onsager frequencies are absent in DOS, but there are integer and half-integer non-Onsager frequencies in the resistance. While qualitatively the results for integer non-Onsager frequencies are consistent with the previous picture of commensurate oscillations, quantitatively our conclusions are somewhat different. The results of this Section explain all known experimental data on the Shubnikov–de Haas effect, but do not explain oscillations observed in the de Haas–Van Alphen effect. In Section IV we calculate the thermodynamic potential of an ideal Fermi gas in a superimposed 1D periodic potential and magnetic field, this is a technical section. Section V addresses electron-electron interactions and explains non-Onsager oscillations observed in the de Haas–Van Alphen effect. The analysis includes the temperature dependence of the amplitude of the oscillations. Section VI is aimed at chemical potential oscillations in a gated 2DEG. This mechanism leads to non-Onsager oscillations in free energy, however, it does not explain the observed temperature dependence of the effect. In Section VII we consider half-frequency non-Onsager oscillations due to impurities. This effect conceptually has a distant similarity to the Al'tshuler-Aronov-Spivak effect [24]. Section VIII presents our conclusions.

II. MOTION IN A ONE-DIMENSIONAL PERIODIC POTENTIAL

A. Energy levels

Our results are generic, however, for the sake of presentation we work with a specific potential: the one-dimensional sinusoidal potential.

$$U(x) = 2W \cos(gx) \quad (1)$$

This potential is imposed on a two-dimensional electron gas (2DEG) with quadratic dispersion, $\varepsilon(\mathbf{p}) = \frac{p^2}{2m}$. We assume that both the potential modulation and the magnetic field are small compared to the Fermi energy, $W, \hbar\omega \ll \varepsilon_F$, so that the semi-classical approximation is valid. The semi-classical trajectory of a free electron is a circle in momentum space (Fig. 1a); the sign of the magnetic field corresponds to clockwise propagation. Diffraction from the potential, Eq. 1, makes the “trajectory” periodic in k_x (see Fig. 2, the propagation remains clockwise). Note that Fig. 2 corresponds to the case $g/2 < p_F < g$.

We put the term “trajectory” in inverted commas because this is not quite a classical trajectory, there are quantum mechanical jumps at the Brillouin zone boundaries. For a trajectory without jumps the wave-function

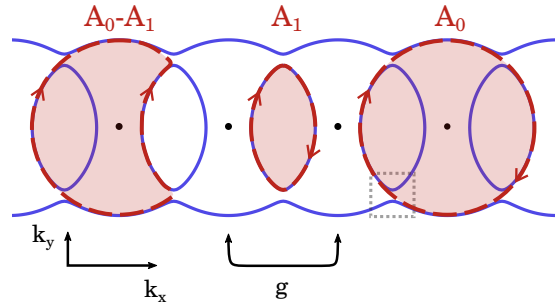


Figure 2. Blue lines show Fermi surface of a 2DEG with a one-dimensional periodic potential (Eqn. 1). Red lines show Semi-classical electron “trajectories” with arrows indicating the direction of motion.

in the semi-classical approximation is $\psi(\mathbf{p}) \propto e^{iS(\mathbf{p})}$, where $S(\mathbf{p})$ is the phase (action) along the trajectory, though the approximation fails where two circular trajectories intersect. An intersection point is shown in Fig. 3a. We can describe quantum mechanical jumps by a scattering matrix S , relating incoming waves 1 and 3 to “reflected” waves 2 and 4.

$$\hat{S} \begin{pmatrix} 1 \\ 3 \end{pmatrix} = \begin{pmatrix} 4 \\ 2 \end{pmatrix} \quad \hat{S} = \begin{pmatrix} S_{41} & S_{43} \\ S_{21} & S_{23} \end{pmatrix} = \begin{pmatrix} s & ce^{-i\varphi} \\ -ce^{i\varphi} & s \end{pmatrix} \quad (2)$$

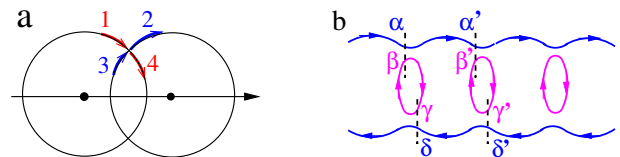


Figure 3. (a) Scattering states for a quantum mechanical jump between two orbits. (a) Definition of wave amplitudes at different points along the semi-classical trajectory. Unprimed letters are separated from primed letters by a momentum $(g, 0)$.

Since \hat{S} is unitary the parameters c and s are real with $c^2 + s^2 = 1$. In the perturbative limit, $W \rightarrow 0$, the wave 1 scatters to 4 and the wave 3 scatters to 2 (see Fig. 3). Hence, in this case, we must have $s \rightarrow 1$ and $c \rightarrow 0$ (it turns out that $\varphi \rightarrow \pi/4$ also). In the opposite limit, the adiabatic limit, in which W is large the wave 1 scatters to 2 and the wave 3 scatters to 4. Thus, $s \rightarrow 0$, $c \rightarrow 1$ and $\varphi \rightarrow 0$. The explicit scattering matrix is derived in the appendix in terms of the parameters over our problem: the magnetic field, B , the potential amplitude, W , the Fermi momentum, p , and the reciprocal lattice vector g .

$$\begin{aligned}
s &= e^{-\pi z} \\
c &= \sqrt{1 - s^2} \\
\varphi &= \frac{\pi}{4} - \arg(\Gamma(1 + iz)) + z(\ln(z) - 1) \\
z &= \frac{W^2}{2(\omega \epsilon g/p) \sqrt{1 - g^2/4p^2}}
\end{aligned} \tag{3}$$

Here $\omega = \frac{eB}{m}$ is the cyclotron frequency and $\epsilon = p^2/2m$ is the energy of the electron. We are mostly interested in the case $g \sim p$, so the perturbative limit corresponds to $W \ll \sqrt{\omega \epsilon}$ and the adiabatic limit corresponds to $W \gg \sqrt{\omega \epsilon}$. We use the term “magnetic breakdown regime” to refer to the intermediate case $W \sim \sqrt{\omega \epsilon}$. Of course, we always assume that W and ω are much less than ϵ . Eqns. 2 and 3 fully describe scattering around the intersection of two circular orbits.

Next, we account for the periodicity of Fig. 2. In Fig. 3b we denote by Greek letters the wave functions at the point on the trajectory just before scattering. The primed points are separated from the un-primed points by one period, g . According to Bloch’s theorem the wave functions are related by

$$\begin{aligned}
\alpha' &= e^{ik} \alpha \\
\beta' &= e^{ik} \beta \\
\gamma' &= e^{ik} \gamma \\
\delta' &= e^{ik} \delta
\end{aligned} \tag{4}$$

Where e^{ik} is a phase factor and k is the “quasi-momentum”. Free, semi-classical propagation away from the intersections is described by the matrix

$$\hat{P} = \begin{pmatrix} P_m & 0 \\ 0 & P_b \end{pmatrix} \tag{5}$$

Here $P_b = e^{iS_b}$ describes propagation along the blue line in Fig. 3b from α to α' or from δ' to δ . And $P_m = e^{iS_m - i\pi/2}$ describes propagation along half of the magenta oval in Fig. 3b. Each half of this oval contains a classical turning point, leading to the caustic phase $\pi/2$ in P_m . The actions S_b and S_m are related to the areas A_0 and A_1 introduced above as

$$\begin{aligned}
S_m &= \frac{A_1}{2|eB|} \\
S_b + S_m &= \frac{A_0}{2|eB|}
\end{aligned} \tag{6}$$

Combining scattering events and propagations gives a relation between the amplitudes defined in Fig. 3

$$\begin{pmatrix} \gamma \\ \alpha' \end{pmatrix} = \hat{P} \hat{S} \begin{pmatrix} \alpha \\ \beta \end{pmatrix} \\
\begin{pmatrix} \beta' \\ \delta \end{pmatrix} = \hat{P} \hat{S} \begin{pmatrix} \delta' \\ \gamma' \end{pmatrix}
\end{aligned} \tag{7}$$

Equations 4 and 7 are a system of four equations with four coefficients: $\alpha, \beta, \gamma, \delta$. The right hand side of this system of equations is zero meaning that non-trivial solutions occur only when the determinant is equal to zero. In a simplified form this condition reads

$$\begin{aligned}
0 &= \cos\left(\frac{A_0}{2|eB|}\right) + 2c \cos(k) \cos\left(\frac{A_1}{2|eB|} - \varphi\right) + \\
&\quad c^2 \cos\left(\frac{A_0 - 2A_1}{2|eB|} + 2\varphi\right)
\end{aligned} \tag{8}$$

The areas A_0 and A_1 can be found explicitly in the limit $W \rightarrow 0$.

$$\begin{aligned}
A_0 &= \pi p^2 \\
A_1 &= 2p^2 \arcsin \sqrt{1 - \frac{g^2}{4p^2}} - gp \sqrt{1 - \frac{g^2}{4p^2}}
\end{aligned} \tag{9}$$

These areas, as well as the parameters of the scattering matrix (Eq. 3), depend on the energy, $\epsilon = p^2/2m$. Eq. 8 is therefore a highly nonlinear function of energy which allows us to find the energy levels, $\epsilon_{n,k}$, of the system at a given magnetic field, B . The energy levels depend on an integer quantum number n that originates from the Landau level index and on the continuous parameter k limited by $-\pi < k < +\pi$. Eq. 8 can be solved analytically in certain simple cases; that is, when $c = 0$ or $c = 1$.

The approach described above was developed by Pippard in Ref. [25]. However, the Pippard work derives Eq. 8 without account of the reflection phase, φ .

B. Density of states in the weak scattering limit.

The density of states, ρ , is the simplest equilibrium property containing magnetic oscillations. We present an explicit calculation of the oscillating components of ρ in this section as an instructive example which leads on to our later calculations of the thermodynamic potential. Our expression for ρ contains some of the essential features of the problem: the lack of non-Onsager frequencies in the single particle picture. Importantly, this calculation cannot address the temperature dependence of magnetic oscillations; that requires a study of the full thermodynamic potential.

We consider the quantization condition (Eq. 8) analytically in the limit of weak scattering, $W^2 \ll \omega \epsilon$, which is realised in the experiment Ref. [8]. In this limit c is a small parameter, so we can solve Eq. 8 perturbatively, in powers of c . Here, as well as in the rest of analytical

calculations in this paper, we work to second-order in c . First, the zeroth order solution ($c = 0$) of Eq. 8 gives usual Landau levels.

$$\epsilon_n^{(0)} = \omega(n + 1/2) \quad (10)$$

Where $n = 0, 1, 2, \dots$. The degeneracy of each Landau level arises from the free parameter k . The solution of Eq. 8 to second order in c is straightforward, it depends on the energy derivatives, $A' = \partial A / \partial \epsilon$, and on the areas, A , each of which must be evaluated at $\epsilon = \epsilon_n^{(0)}$. In particular, $A_0 = 2\pi m \omega(n + 1/2)$ and $A'_0 = 2\pi m$. To second-order in c the parameters of the scattering matrix (Eq. 3) are

$$\begin{aligned} s &\approx 1 - c^2/2 \\ \varphi &\approx \frac{\pi}{4} - \frac{c^2}{2\pi} \left(\ln \frac{2\pi}{c^2} + 0.42 \right) \end{aligned} \quad (11)$$

And the solution of Eq. 8 for the energy levels, $\epsilon_{n,k}$, is

$$\begin{aligned} \epsilon_{n,k} &= \epsilon_n^{(0)} + \delta\epsilon_{n,k} \\ \delta\epsilon_{n,k} &= \frac{2\omega}{\pi} c \cos(k) \sin \left(\frac{A_0 - A_1}{2|eB|} + \varphi \right) + \\ &\quad \frac{\omega}{\pi} c^2 \sin \left(\frac{A_1}{|eB|} - 2\varphi \right) \left[1 - 2 \frac{A'_1}{A'_0} \cos^2 k \right] \end{aligned} \quad (12)$$

The degeneracy of each Landau level is lifted due to the quasi-momentum, k .

We can obtain the density of states from this expression using

$$\rho(\epsilon, B) = \sum_n \int_{-\pi}^{\pi} \delta(\epsilon - \epsilon_{n,k}) \frac{dk}{2\pi} \quad (13)$$

The above solution implies that the magnetic field is fixed and energy is variable. We can also fix the energy equal to the chemical potential, $\epsilon = \mu = \epsilon_F$, and vary the magnetic field. This representation is more convenient for magnetic oscillations. In this case the areas $A_0 = A_0(\mu)$ and $A_1 = A_1(\mu)$ in Eq. 8 are fixed, but magnetic field varies. The density of states at the Fermi energy is then

$$\rho(B) \propto \sum_{n,k} \delta(B - B_{n,k})$$

Where $B_{n,k}$ are solutions to Eq. 8. Hereafter we assume that $B > 0$ and omit the absolute value in $|eB|$. Repeating the second-order expansion of Eq. 8 in this representation gives

$$\begin{aligned} \frac{A_0}{eB_{n,k}} &= 2\pi(n + 1/2) \\ &+ 4c \cos(k) \sin [\pi(1 - \gamma)(n + 1/2) + \varphi] \\ &+ (2c^2(1 - 2\gamma \cos^2(k)) \sin [2\pi\gamma(n + 1/2) - 2\varphi] \\ \gamma &= \frac{A_1}{A_0} \end{aligned} \quad (14)$$

Magnetic oscillations are periodic in $1/B$, we address oscillations by taking the Fourier transform of the density of states with respect to $1/B$.

$$\rho_q = \int e^{iq/B} \rho(B) d(1/B) \propto \sum_{n,k} e^{iq/B_{n,k}} \quad (15)$$

We substitute $1/B_{n,k}$ from Eq. 14 to obtain

$$\begin{aligned} \rho_q &\propto \sum_n e^{i2\pi Q(n+1/2)} \times \\ &\quad [(1 - 2c^2 Q^2) \\ &\quad - c^2 Q(1 - \gamma + Q) e^{-i2\pi\gamma(n+1/2)+2i\varphi} \\ &\quad + c^2 Q(1 - \gamma - Q) e^{+i2\pi\gamma(n+1/2)-2i\varphi}] \end{aligned} \quad (16)$$

Where

$$Q = \frac{q}{|e|A_0}$$

We remind that the convention is for frequency to be positive, $Q > 0$. Eqn. 16 contains several harmonics:

1. The second line in Eq. 16 gives a peak in the Fourier transform at integer Q , leading to frequencies $q = eA_0 n$ for $n = 1, 2, \dots$. This is the usual Onsager frequency for A_0 ; its amplitude, $1 - 2c^2 n^2$, is non-zero even at $c = 0$.
2. The third line in Eq. 16 gives a Fourier peak when $Q - \gamma = n$ for $n = 0, 1, 2, \dots$. In terms of the frequency we have $q = eA_0 n + eA_1$. In particular, this harmonic leads to $q = eA_1$ and to $q = e(A_0 + A_1)$. The corresponding amplitudes are proportional to c^2 .
3. The fourth line in Eq. 16 gives a Fourier peak when $Q + \gamma = n$ for $n = 0, 1, 2, \dots$ or $q = eA_0 n - eA_1$. From this harmonic we obtain the Onsager frequency $q = e(2A_0 - A_1)$. Notably, this condition also allows for the non-Onsager frequency $q = e(A_0 - A_1)$ when $Q + \gamma = 1$. However, computing the amplitude of this harmonic, $c^2 Q(1 - Q - \gamma)$, gives exactly zero.

Thus, the density of states oscillates with a variety of different Onsager frequencies. Non-Onsager frequencies are notably not present.

The above analytical analysis is valid up to the second order in c . To verify our conclusion in any order in c we solve Eq. 8 exactly numerically. Here we present results for GaAs with $m = 0.07m_e$, the Fermi energy $\epsilon_F = 8$ meV (corresponds to the density $n = 2.36 \times 10^{11} \text{ cm}^{-2}$), the superlattice spacing $a = 80$ nm, and the tunneling matrix element $c = 0.6$. The Fourier transform of the DOS versus frequency f is plotted in Fig. 4. The frequency has dimension Tesla and is defined as $q = 2\pi f$, see Eq. 15. The Fourier transform shows peaks at A_0 ($f = 4.85$ T), A_1 , and various combinatorial frequencies, however, there are no peaks at non-Onsager frequencies.

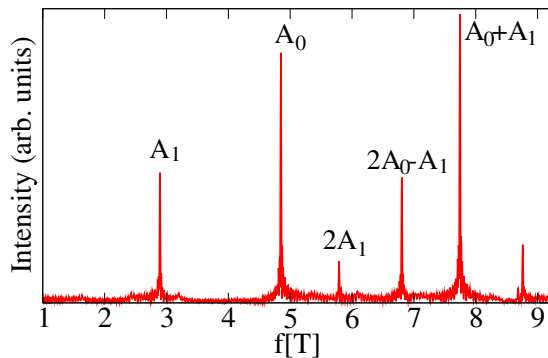


Figure 4. Fourier transform of the density of states vs frequency obtained by numerical solution of Eq. 8. There are peaks at A_0 ($f = 4.85$ T), A_1 , and at combinatorial frequencies, but there are no peaks at non-Onsager frequencies. The parameters are $\epsilon_F = 8$ meV, $a = 80$ nm, $c = 0.6$.

III. EXACT NUMERICAL SOLUTION OF THE SINGLE PARTICLE SCHRÖDINGER EQUATION

In the present section we solve exactly numerically the single particle Schrödinger equation using the KWANT software package [26]. The important point is that the package allows us to calculate the density of states and multi-terminal resistances, meaning it can address both equilibrium and non-equilibrium properties of the system. The aim of the present section is twofold: first, to check by another method (KWANT) that ρ does not contain non-Onsager oscillations, and second, to check that the resistance—a non-equilibrium property—contains non-Onsager oscillations and hence to demonstrate a correspondence with previous works based on the semi-classical kinetic equation [12, 17–19].

We solved the quantum mechanical problem of electron scattering for a two-dimensional system with either a one-dimensional or a two-dimensional potential modulation. A schematic of the device is shown in Fig. 5. The lattice potential is defined in the central square, on each side of which there are two horizontal channels. Electrons incident on the lattice from one channel are scattered into the three other channels. Calculations were performed for devices containing 40 to 50 lattice periods. In the schematic (Fig. 5), the vertical lines show a one-dimensional modulation of potential along x , with the current between contacts 1 and 2 directed perpendicular to the equipotential lines. The magnetic field is directed perpendicular to the 2D plane.

KWANT calculates the density of states and four-terminal transmission coefficients for given values of energy ϵ_F and magnetic field B . Four-terminal resistances are determined from the calculated transmission coefficients within the framework of the Landauer-Büttiker formalism [27]. We then apply a Fourier transform to the calculated $\rho(1/B)$ and $R_{xx}(1/B)$ in order to determine the characteristic frequencies.

We consider first the one-dimensional potential de-

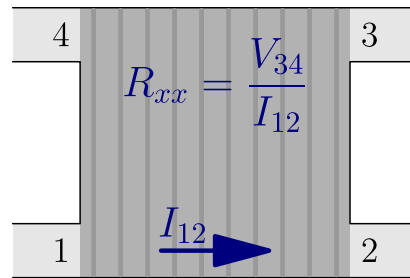


Figure 5. Schematic of the four-terminal device simulated using KWANT. One-dimensional potential modulation along x is shown by vertical lines.

scribed by Eqn. 1. In the case of an 80 nm period the potential is defined on a square mesh with the mesh spacing 8 nm. To remove interference fluctuations related to scattering from the device boundaries we introduce a random disorder $-V_r/2 < V < V_r/2$ on every site of the mesh [28, 29].

In Fig. 6 we present the results of our KWANT calculation for the same parameters used in Fig. 4: the Fermi energy $\epsilon_F = 8$ meV (corresponding to a density $n = 2.36 \times 10^{11} \text{ cm}^{-2}$), the superlattice period $a = 80$ nm, and the superlattice amplitude $W = 0.4$ meV. The density of states is given by the red line in Fig. 6 and shows perfect agreement with the results of the semi-classical calculation (Fig. 4). In particular the density of states contains only Onsager frequencies. The resistance, however, manifests the non-Onsager frequency $A_0 - A_1$ in addition to other Onsager frequencies (blue line in Fig. 6).

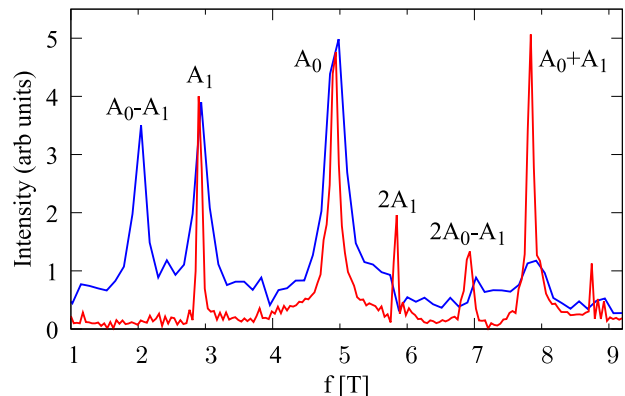


Figure 6. Fourier transforms of ρ (red) and R_{xx} (blue) vs frequency for a one-dimensional superlattice. The results are obtained using KWANT. The parameters are $\epsilon_F = 8$ meV, $a = 80$ nm, $W = 0.4$ meV, $V_r = 0.5$ meV.

The presence of the non-Onsager line $A_0 - A_1$ in the resistance is consistent with previous results using kinetic equation theory [12, 17–19], however, there is a difference. According to the semi-classical theory [17–19] the period of oscillations is determined by the condition that the diameter of the cyclotron orbit is equal to an integer num-

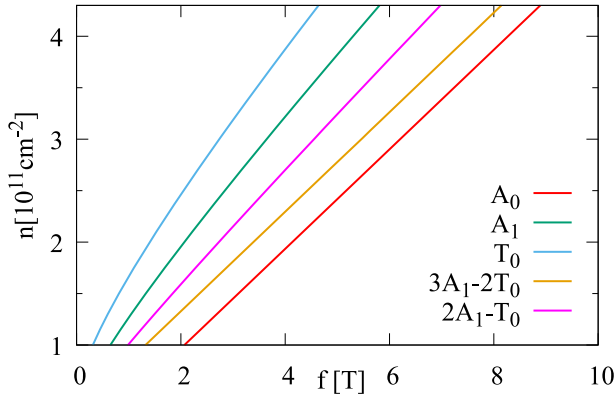


Figure 7. Fourier peaks of density of states ρ for a 2D triangular modulation. Lines indicate positions of the Fourier transform peaks on the density-frequency plane. The potential amplitude is $W = 0.3$ meV, the amplitude of disorder is $V_r = 1$ meV. Only Onsager frequencies are observed in ρ .

ber of lattice periods, this is why quite often these oscillations are called "commensurability oscillations". This condition gives the frequency of oscillations

$$f = \frac{g p_F}{\pi} \quad (17)$$

According to our calculation the frequency is

$$f = \frac{A_0 - A_1}{2\pi}, \quad (18)$$

where A_0 and A_1 are given by Eqn. 9. While in the classical limit ($g \ll p_F$) Eqns. 17 and 18 are identical, at $g \rightarrow 2p_F$ the approximate commensurability expression (Eqn. 17) differs from the exact one (Eqn. 18) by 27%.

We have also used KWANT to study a two-dimensional triangular potential

$$U(\mathbf{r}) = 2W [\cos(\mathbf{g}_1 \cdot \mathbf{r}) + \cos(\mathbf{g}_2 \cdot \mathbf{r}) + \cos(\mathbf{g}_3 \cdot \mathbf{r})] \quad (19)$$

Here \mathbf{g}_i are the basic vectors of the honeycomb Brillouin zone. We use the same lattice spacing as for the 1D modulation, $a = 80$ nm, and the same as that in the experimental work Ref. [8]. Fig. 7 presents our results for ρ : positions of the Fourier transform peaks on the density-frequency plane. Since there are a larger number of possible orbits on the triangular lattice, we present the dependence of frequency on density for each Fourier peak, which allows us to pin down exactly which orbit corresponds to which line. Again, only Onsager frequencies are observed in ρ , the corresponding trajectories are marked for every line, some of these trajectories are related to the triangular orbit T_0 shown in Fig.8.

Fig. 9 presents our results for resistance: similar to Fig. 7 we plot the central frequency of each Fourier peak as a function of density. Similar to what we observed for a 1D superlattice the resistance manifests non-Onsager frequencies (several of them, including $A_0 - A_1$), moreover, it even manifests half-frequencies

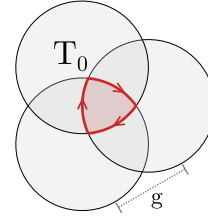


Figure 8. Triangular electron trajectory T_0 –due to magnetic breakdown in a triangular periodic potential (Eqn. 19).

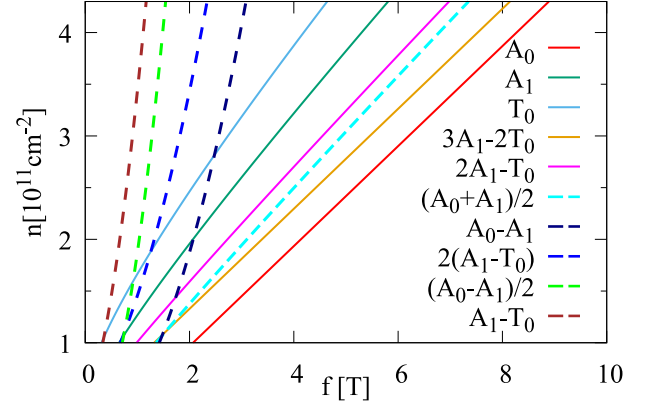


Figure 9. Nonlocal resistance R_{xx} for 2D triangular modulation: positions of the Fourier transform peaks on the density-frequency plane. The potential amplitude $W = 0.3$ meV, the amplitude of disorder $V_r = 1$ meV. Onsager lines are solid and non-Onsager ones are dashed.

(e.g. $(A_0 - A_1)/2$). These non-Onsager frequencies are indicated by the dashed lines in Fig. 9; the solid lines show Onsager frequencies that were also observed in the density of states.

The numerical results of this section explain all existing transport experiments, including the most recent one, Ref. [8]. In other words, our numerics fully explain the Shubnikov–de Haas effect in the magnetic breakdown regime. However, as we pointed out in the introduction, non-Onsager oscillations have been also observed in the equilibrium de Haas–Van Alphen effect [16, 21] and any kinetic mechanisms are irrelevant in this case. The rest of this paper is concerned with the equilibrium case. To address this case we need to consider the thermodynamic Ω -potential.

IV. THERMODYNAMIC POTENTIAL OF NON INTERACTING (IDEAL) ELECTRON GAS

Thus far we have shown that non-Onsager frequencies *cannot* appear in the density of states. We turn now to our result related to the interaction: non-Onsager frequencies arise due to Coulomb electron-electron interactions. This is the only mechanism that contributes to the de Haas–Van Alphen effect, of course the mechanism also

contributes to the Shubnikov–de Haas effect. Specifically, it will be shown that an $A_0 - A_1$ frequency appears in the thermodynamic potential, Ω , with the correct temperature dependence.

We present two calculations; instead of dealing with magnetisation directly we deal with Ω . First, in this section, we calculate Ω without Coulomb interactions. This result reiterates the results of the previous section and introduces our basic technique. Second, in the following section, we calculate the correction $\delta\Omega$ to the thermodynamic potential due to a repulsive contact interaction between electrons. This correction contains non-Onsager frequencies.

The thermodynamic potential has of course already been computed in a general form by Lifshitz and Kosevich[30], however, the calculation does not include both magnetic breakdown and Coulomb interactions. To account for magnetic breakdown we make use of the energies Eq. (8) obtained within the Pippard model. Coulomb interactions are accounted for in the following section using a technique which builds on the one developed here.

The Ω -potential of an ideal gas with a set of energy levels $\varepsilon_{n,k}$ is given by

$$\Omega = -T \frac{eB}{\pi} \sum_{n,k} \ln \left(e^{(\mu - \varepsilon_{n,k})/T} + 1 \right) \quad (20)$$

$$\propto \int d\varepsilon \rho(\varepsilon, B) \ln \left(e^{(\mu - \varepsilon)/T} + 1 \right)$$

This is a linear functional of the density of states, $\rho(\varepsilon, B)$; since the non-Onsager frequencies are absent from ρ they must also be absent from Ω . Note that we normalize the k -integration as $\sum_k = 1$. The contribution of each Landau level must therefore be multiplied by the capacity of the level eB/π .

We compute Ω up to second order in the breakdown amplitude c using Eqn.(12): $\varepsilon_{nk} = \varepsilon_n^{(0)} + \delta\varepsilon_{nk}$. The calculation consists of 4 steps. (i) First expand the logarithm in the 1st line of Eq. (20) up to the second order in $\delta\varepsilon_{nk}$. Starting from $F(\varepsilon_{nk}) = \ln(e^{(\mu - \varepsilon_{nk})/T} + 1)$ we obtain

$$F(\varepsilon_{nk}) = F(\varepsilon_n^{(0)}) + \frac{\partial F}{\partial \varepsilon} \delta\varepsilon_{nk} + \frac{1}{2} \frac{\partial^2 F}{\partial \varepsilon^2} \delta\varepsilon_{nk}^2 \quad (21)$$

After this expansion the integration over k is performed, eliminating the linear in c term (see Eqn. 12). (ii) Next, in each term of Eqn. 21 we replace summation over n by integration over x using the Poisson formula.

$$\sum_{n=0}^{\infty} \bar{F}(n) = \frac{1}{2} \bar{F}(0) + \int_0^{\infty} \bar{F}(x) dx + 2Re \sum_{l=1}^{\infty} \int_0^{\infty} \bar{F}(x) e^{2\pi i l x} dx \quad (22)$$

Here $\bar{F}(n)$ represents $\sum_k F(\varepsilon_{n,k})$. So, the discrete index n is replaced by the continuous variable x . (iii) In the 3rd

step we perform, if necessary, the x -integration by parts to bring the Fermi-Dirac distribution to the bell-shape function peaked at the chemical potential.

$$\frac{e^{(\varepsilon_x^{(0)} - \mu)/T}}{\left(e^{(\varepsilon_x^{(0)} - \mu)/T} + 1 \right)^2}$$

(iv) In the final step we perform the integration over x using

$$\int_{-\infty}^{+\infty} e^{i\alpha x} \frac{e^x}{(e^x + 1)^2} = \frac{\pi\alpha}{\text{sh}(\pi\alpha)}$$

This calculation results in the following Ω -potential.

$$\Omega = -\frac{m}{2\pi} \mu^2 - \frac{m\omega^2}{2\pi^3} \left[\frac{t_0}{\text{sh}(t_0)} \cos\left(\frac{A_0}{eB}\right) + \frac{c^2}{\alpha} \frac{t_1}{\text{sh}(t_1)} \cos\left(\frac{A_1}{eB} - 2\varphi\right) \right] \quad (23)$$

Where

$$t_0 = \frac{dA_0}{d\varepsilon} \frac{\pi T}{eB} = 2\pi^2 T/\omega$$

$$t_1 = \frac{dA_1}{d\varepsilon} \frac{\pi T}{eB} = \alpha 2\pi^2 T/\omega$$

$$\alpha = \frac{dA_1}{d\varepsilon} \bigg/ \frac{dA_0}{d\varepsilon}$$

The first term in the oscillating part of the Ω -potential is the usual Lifshitz-Kosevich expression, and the second term corresponds to the A_1 -frequency. The temperature dependence of the A_1 -term is different from that of the A_0 -term. As we explained the non-Onsager frequency $A_0 - A_1$ does not appear. Of course, there are terms with other Onsager frequencies, we just do not present them.

V. THERMODYNAMICS POTENTIAL WITH ELECTRON-ELECTRON INTERACTIONS

One of our main results is that the inclusion of electron-electron interactions leads to a finite amplitude for non-Onsager frequencies with the correct temperature dependence. We stress that this is an entirely equilibrium effect. While the calculation is somewhat involved the procedure is straightforward: we substitute the energy levels obtained from the Pippard model into the leading interaction correction to the Ω -potential and then expand to second order in the magnetic breakdown parameter, c .

With account of screening the electron-electron Coulomb interaction in momentum space reads

$$\frac{2\pi e^2}{q - 2\pi e^2 P_q} \rightarrow \frac{2\pi e^2}{q + 2me^2} \rightarrow \frac{\pi}{m} \quad (24)$$

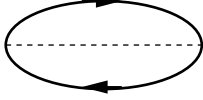
Here we take into account that at a relevant momentum transfer, $q < 2p_F$, the polarization operator is

$P_q = -m/\pi$, and also neglect q compared to $2me^2$. Transferring (24) to the coordinate representation we get the repulsive contact interaction

$$\begin{aligned} H_{int} &= \lambda \delta(\vec{r}_1 - \vec{r}_2) \\ \lambda &= \frac{\pi}{m} \end{aligned} \quad (25)$$

The leading-order interaction correction to the Ω -potential is given by the exchange diagram in Fig. 10.

Figure 10. Diagram for the leading-order interaction correction to Ω . Solid lines represent electrons. The dashed line represents the Coulomb interaction.



The correction shown in Fig. 10 is given explicitly by [31]

$$\begin{aligned} \delta\Omega &= -\frac{1}{2} \sum_{ij} \langle \psi_j^*(r_1) \psi_i^*(r_2) | H_{int} | \psi_i(r_1) \psi_j(r_2) \rangle f_i f_j \\ f_i &= \frac{1}{e^{(\epsilon_i - \mu)/T} + 1} \end{aligned} \quad (26)$$

Here, the indices i and j enumerate quantum states; the index describes both orbital motion and spin. In what follows we skip spin and accordingly skip the pre-factor $1/2$ in (26). Without magnetic field and at $T = 0$ the correction can be immediately calculated using plane-wave quantum states, $\psi_i \propto e^{i\mathbf{p}_i \cdot \mathbf{r}}$.

$$\delta\Omega(B = 0, T = 0) = -\frac{1}{4} \lambda n^2 = -\frac{m}{4\pi} \mu^2 \quad (27)$$

This correction is just two times smaller than the first term in Eq. (23). We are interested in non-zero magnetic fields, however, and in this case the wave-functions depend on gauge. We work with vector potential $A = (0, Bx, 0)$, so the single electron wave-function is

$$\psi_{nk} = e^{iky} \chi_n(x + k/eB) \quad (28)$$

Where χ_n is the oscillator wave function corresponding to the Landau level n . We reiterate that in the 1D model (Eq. 1) the potential is modulated along the x -direction so that k in Eq. 28 remains a good quantum number in the presence of the periodic potential. Note that the k which arises in the wave-function (Eqn. 28) differs from the dimensionless k in the semi-classical expression for energy levels (Eqn. 12). In terms of the k from Eqn. 28, the dimensionless parameter in Eqn. 12 is given by gk/eB .

Now, we can rewrite the exchange correction to Ω (Eqn. 26) as

$$\delta\Omega = -\frac{eB}{2\pi} \sum_{n_1, k_1, n_2, k_2} V_{n_1, k_1, n_2, k_2} f_{n_1, k_1} f_{n_2, k_2} \quad (29)$$

Where V is the exchange matrix element of the interaction and is given by

$$\begin{aligned} V_{n_1, k_1, n_2, k_2} &= \lambda \int dx \chi_{n_1}^2(x) \chi_{n_2}^2(x + q/eB) \\ q &= k_1 - k_2 \end{aligned} \quad (30)$$

The pre-factor in Eq. 29 is fixed by evaluating this expression at $T = 0$ with neglect of $\delta\epsilon_{nk}$ and then comparing with the result of Eq. 27 (found using plane-waves).

In the following calculation it is convenient to define the average matrix element $V^{(0)}$

$$\begin{aligned} V_{n_1, n_2}^{(0)} &= \sum_q V_{n_1, k_1, n_2, k_2} \\ &= \lambda \int dx \chi_{n_1}^2(x) \chi_{n_2}^2(x + x_q) \frac{dq}{2\pi} \\ &= \lambda \frac{eB}{2\pi} \end{aligned} \quad (31)$$

Here $x_q = \frac{q}{eB}$. Similarly we define $V^{(1)}$,

$$\begin{aligned} V_{n_1, n_2}^{(1)} &= \sum_q V_{n_1, k_1, n_2, k_2} \cos(x_q g) \\ &= \lambda \int dx \frac{dq}{2\pi} \chi_{n_1}^2(x) \chi_{n_2}^2(x + x_q) \cos(x_q g) \\ &= \lambda \frac{eB}{2\pi} M_{n_1} M_{n_2} \\ M_n &= L_n(l_B^2 g^2 / 2) e^{-l_B^2 g^2 / 4} \end{aligned} \quad (32)$$

Here $g = 2\pi/a$ is the reciprocal vector of the potential modulation (Eq. 1), $l_B = 1/\sqrt{eB}$ is the magnetic length and L_n is a Laguerre polynomial. Note that in the limit of large n we have $M_n \rightarrow J_0(\sqrt{2n} l_B g)$.

Next we compute the oscillating part of $\delta\Omega$. Following the procedure used in the previous section for the ideal gas, we expand $\delta\Omega$ (Eq. 29) up to second order in c using the energy levels $\epsilon_{n,k} = \epsilon_n^{(0)} + \delta\epsilon_{n,k}$ (see Eq. 12). Expanding the Fermi-Dirac distribution up to second order in $\delta\epsilon_{n,k}$ gives

$$f(\epsilon_{nk}) = f(\epsilon_n^{(0)}) + f'(\epsilon_n^{(0)}) \delta\epsilon_{n,k} + \frac{1}{2} f''(\epsilon_n^{(0)}) \delta\epsilon_{n,k}^2 \quad (33)$$

This expression can then be substituted into Eqn. 29 for $\delta\Omega$. Performing the integration over k introduces terms involving $\bar{f}_n \equiv \sum_k f(\epsilon_{n,k})$ and transforms Eq. 29 into

$$\delta\Omega = -\frac{eB}{2\pi} \sum_{n_1, n_2} \left[V_{n_1, n_2}^{(0)} \bar{f}_{n_1} \bar{f}_{n_2} + V_{n_1 n_2}^{(1)} \frac{2c^2\omega^2}{\pi^2} f'(\varepsilon_{n_1}^{(0)}) f'(\varepsilon_{n_2}^{(0)}) \sin\left(\frac{A_0 - A_1}{2eB} + \varphi\right)_{n_1} \sin\left(\frac{A_0 - A_1}{2eB} + \varphi\right)_{n_2} \right] \quad (34)$$

$$\bar{f}_n = \sum_k f(\varepsilon_{n,k}) = f(\varepsilon_n^{(0)}) + f'(\varepsilon_n^{(0)}) \frac{c^2\omega}{\pi} (1 - \alpha) \sin\left(\frac{A_1}{eB} - 2\varphi\right)_n + f''(\varepsilon_n^{(0)}) \frac{c^2\omega^2}{\pi^2} \sin^2\left(\frac{A_0 - A_1}{2eB} + \varphi\right)_n$$

Thus, $\delta\Omega$ reduces to a sum of two parts: one due to $V_{n_1, n_2}^{(0)}$ and another due to $V_{n_1, n_2}^{(1)}$. Since $V_{n_1, n_2}^{(0)}$ is independent of n_1 and n_2 (see Eq. 31), the summations over n_1 and n_2 in the corresponding term of Eq. 34 are independent. From $V^{(0)}$ we obtain the following contribution to $\delta\Omega$.

$$\delta\Omega = -\frac{eB}{\pi} V^{(0)} \left(\sum_n \bar{f}_n \right)^2$$

$$\sum_n \bar{f}_n = \frac{\mu}{\omega} - \frac{t_0/\pi}{\text{sh}(t_0)} \sin\left(\frac{A_0}{eB}\right) - \frac{c^2 t_1/\pi}{\text{sh}(t_1)} \sin\left(\frac{A_1}{eB} - 2\varphi\right) \quad (35)$$

The second line is obtained using the Poisson summation rule and A_0 and A_1 are taken at the chemical potential. Note that the parameters t_0 and t_1 are defined in Eq. (23). Thus, upon squaring $\sum_n \bar{f}_n$ we obtain combinations of the A_0 , A_1 , and zero frequencies. This gives the interaction correction to the standard Onsager frequencies, A_0 and A_1 , present in the ideal gas. More importantly, however, it leads to the non-Onsager frequency $A_0 - A_1$.

$$\delta\Omega^{(0)} \rightarrow -\frac{\lambda c^2 m^2 \omega^2}{4\pi^4} \frac{t_0}{\text{sh}(t_0)} \frac{t_1}{\text{sh}(t_1)} \cos\left(\frac{A_0 - A_1}{eB} + 2\varphi\right) \quad (36)$$

The non-Onsager frequency appears because the interaction contribution is a non-linear functional of the single-particle density of states (see Eq. 29). This non-linearity gives rise to combinations of the frequencies which ordinarily appear in the density of states. Note, however, that the frequency $A_0 - A_1$ should disappear at the same temperature as A_0 according to the above equation. The term given in Eqn. 36 cannot explain the observed non-Onsager frequencies which survive to ‘high’ temperatures. To resolve this issue we turn to the $V^{(1)}$ term in Eq. 34.

Next, using Poisson formula, we perform the n_1 and n_2 summations in the $V_{n_1 n_2}^{(1)}$ -term in (34). Altogether this results in the following correction to the grand potential.

$$\delta\Omega^{(1)} = -\frac{\lambda c^2 m^2 \omega^2}{2\pi^4} [J_0(p_F g/eB)]^2$$

$$\times \left[\frac{(t_0 - t_1)/2}{\text{sh}((t_0 - t_1)/2)} \sin\left(\frac{A_0 - A_1}{2eB} + \varphi\right) \right]^2 \quad (37)$$

We have evaluated M_n at $n \approx \mu/\omega \gg 1$ in which case $M_n \approx J_0(p_F g/eB)$ (for Fermi momentum $p_F = \sqrt{2m\mu}$). This interaction correction is another contribution to non-Onsager quantum magnetic oscillations. At zero temperature, $t_0, t_1 \rightarrow 0$, the contribution from $V^{(1)}$ (Eq. 37) is suppressed relative to the contribution from $V^{(0)}$ (Eq. 36) by the factor $[J_0(p_F g/eB)]^2$. Under the experimental conditions of Ref. [8] this is an order of magnitude suppression. Importantly, however, the two contributions (Eqs. 37 and 36) have a very different temperature dependence. The non-Onsager oscillations in Eq. 37 decay with temperature as $e^{-(t_0 - t_1)} = e^{-2\pi^2(1-\alpha)T/\omega}$. At the same time Onsager oscillations decay as $A_0 : e^{-2\pi^2 T/\omega}$, $A_1 : e^{-2\pi^2 \alpha T/\omega}$. Typically $\alpha \approx 1$ and this explains why the non-Onsager frequency survives till higher temperatures compared to standard Onsager oscillations. For conditions of the experiment [8] at electron density $1 \times 10^{11} \text{ cm}^{-2}$ the amplitude of the $A_0 - A_1$ oscillations decays with temperature 4 times (in exponent) slower than the amplitude of the A_0 oscillation, at density $10 \times 10^{11} \text{ cm}^{-2}$ the ratio is even larger, 6.

To summarise results on the present section. We have computed the leading-order interaction correction to the thermodynamic potential $\delta\Omega$. Our major conclusions are the following. (i) Electron-electron Coulomb interactions explain magnetic oscillations with the non-Onsager frequency $A_0 - A_1$. This works because $\delta\Omega$ is a non-linear functional of the density of states. (ii) The amplitude of the $A_0 - A_1$ frequency decays with temperature much more slowly than that of the standard Onsager frequencies A_0 and A_1 . The interaction mechanism explains $A_0 - A_1$ oscillations observed in the de Haas–Van Alphen effect [16, 21]. Of course, the mechanism also contributes to the Shubnikov–de Haas effect.

VI. THE ROLE OF CHEMICAL POTENTIAL OSCILLATIONS

In this section we return to the non-interacting ideal gas. It is well known that in gated 2D systems the chemical potential is not constant as magnetic field is varied; the electron density is constant instead. Technically, this means that the free energy should be used rather than the grand potential. Practically, this means that the chemical potential oscillates as the magnetic field is varied. Chemical potential oscillations result in non-Onsager magnetic oscillations even without account of

electron-electron interactions [16]. So, to complete our picture of the non-Onsager oscillations, we present here a simple explanation of how this occurs.

The total electron density is fixed and is equal to $n = -\partial\Omega/\partial\mu$. We can thus find an expression for μ by differentiating Eq. 23. This gives

$$\mu = \mu_0 + \delta\mu \quad (38)$$

$$\delta\mu = \frac{\omega}{\pi} \left[\frac{t_0}{\text{sh}(t_0)} \sin\left(\frac{A_0}{eB}\right) + c^2 \frac{t_1}{\text{sh}(t_1)} \sin\left(\frac{A_1}{eB} - 2\varphi\right) \right]$$

That is, the chemical potential can be written as constant part, μ_0 , plus an oscillating part, $\delta\mu$, whose amplitude goes to zero at $B = 0$. Note that μ_0 is proportional to the total electron density and that A_0, A_1 are evaluated at μ_0 . The free energy reads

$$F = \Omega(\mu_0 + \delta\mu) = \Omega(\mu_0) + \delta\mu \partial_{\mu_0}\Omega(\mu_0) \quad (39)$$

According to our equation for the non-interacting free energy (Eqn. 23) we have

$$\partial_{\mu_0}\Omega(\mu_0) = \frac{m\omega}{\pi^2} \left[\frac{t_0}{\text{sh}(t_0)} \sin\frac{A_0}{eB} + c^2 \frac{t_1}{\text{sh}(t_1)} \sin\left(\frac{A_1}{eB} - 2\varphi\right) \right] \quad (40)$$

Hence, the $\delta\mu \partial_{\mu_0}\Omega(\mu_0)$ term in (39) gives the following non-Onsager oscillation of the free energy

$$\delta F = \frac{c^2 m \omega^2}{\pi^3} \frac{t_0}{\text{sh}(t_0)} \frac{t_1}{\text{sh}(t_1)} \cos\left(\frac{A_0 - A_1}{eB} + 2\varphi\right) \quad (41)$$

This frequency arises combinatorially; that is, because, Ω oscillates with a frequency A_1 and μ oscillates with a frequency A_0 . Note that the amplitude is even larger than that of the interaction correction (Eq. 36). However, neither Eq. 41, nor Eq. 36 can explain the temperature dependence of experimental data. The corresponding amplitude decays with temperature almost twice faster than the amplitude of the main harmonic, A_0 . Experimentally, the amplitude of the $A_0 - A_1$ harmonic decays much more slowly than that of A_0 . Only the interaction effect described by Eq. 37 can explain this temperature dependence.

VII. HALF-FREQUENCIES ARISING FROM IMPURITIES

Magnetic oscillations with half-frequencies have been observed for the first time in Ref. [8]. It was conjectured in [8] that the oscillations have the kinetic origin. Results of our Section III confirm that the conjecture was correct, for the triangular lattice half-frequencies arise in transport via the kinetic mechanism. In the present section we demonstrate that the half non-Onsager frequency can arise even in equilibrium in the de Haas–Van Alphen

effect. In this case it is unrelated to the electron-electron interaction, but it is related to impurities.

Our equation for $\varepsilon_n^{(0)} + \delta\varepsilon_{n,k}$ (Eq. 12) gives the energy of a quantum state in a perfect system. While the energy correction contains a term linear in c , none of the magnetic oscillations we have discussed have an amplitude which is linear in c . This is because all linear terms average to zero when we sum over the real quasi-momentum, k .

In the presence of impurities, however, there are also bound states and the quasi-momentum for these states will be imaginary. We obtain the energy of the bound states from Eq. 12 by making the substitutions $k \rightarrow i\kappa$ and $\cos(k) \rightarrow \text{ch}(\kappa)$, where κ is real.

$$\varepsilon_{n,\kappa} = \varepsilon_n^{(0)} + \delta\varepsilon_{n,\kappa}$$

$$\delta\varepsilon_{n,\kappa} = c \frac{2\omega}{\pi} \text{ch}(\kappa) \sin\left(\frac{A_0 - A_1}{2eB} + \varphi\right) \quad (42)$$

To describe the half-frequencies it is sufficient to work to leading-order in c . Note that according to Eq. 42 the energy of the localised impurity state can be above or below the mini-band of a given Landau level, $\varepsilon_{n,k}$, depending on the sign of $\sin((A_0 - A_1)/2eB + \varphi)$. Evidently, it is the presence of this oscillating factor which leads to half-frequencies.

Averaging Eqn. 42 over impurity states we make the replacement $\text{ch}(\kappa) \rightarrow \langle \text{ch}(\kappa) \rangle$, where the average $\langle \text{ch}(\kappa) \rangle$ depends on the concentration of impurities and on the strength of the binding. The most important point is that averages over the mini-band states, $\int \cos(k) dk$, are zero while averages over the impurity states, $\langle \text{ch}(\kappa) \rangle$, are non-zero.

The non-zero average, $\langle \text{ch}(\kappa) \rangle$, means that terms linear in c will appear in both the single-particle density of states and the thermodynamic potential. We focus on the thermodynamic potential, Ω , in particular. Applying the methods of section IV we find that the correction to Ω due to Eqn. 42 is

$$\delta\Omega^{(imp)} = \frac{2cm\omega^2 \langle \text{ch}(\kappa) \rangle}{\pi^3(1-\alpha)} \left[\frac{(t_0 - t_1)/2}{\text{sh}((t_0 - t_1)/2)} \right] \times \cos\left(\frac{A_0 - A_1}{2eB} + \varphi\right) \quad (43)$$

Because of the factor $\langle \text{ch}(\kappa) \rangle$ these oscillations are weak, however, they decay with temperature much more slowly than the main A_0 line, $\propto e^{-(t_0 - t_1)/2} = e^{-\pi^2(1-\alpha)T/\omega}$. These two features – in addition, of course, to the frequency of the oscillations – match the behaviour observed experimentally in Ref. [8]. It is worth noting that the mechanism of the half-frequency $(A_0 - A_1)/2$ discussed in this section is distantly analogous to the AAS effect [24], in which the frequency for Aharonov-Bohm interference is halved due to disorder.

In sense, the frequency described by Eqn. 43 is the fundamental fractional frequency. Given the presence of

$(A_0 - A_1)/2$ other frequencies, such as $(A_0 + A_1)/2$ and $(3A_0 - A_1)/2$, also arise. The additional frequencies appear to first order in c due to the chemical potential oscillations described in the previous section; though in that case their temperature dependence is much stronger than $(A_0 - A_1)/2$ (see the discussion at the end of section VI). These additional half-frequencies were observed in Ref. [8] with a stronger temperature dependence compared to $(A_0 - A_1)/2$.

Since most of the oscillations effects have a geometrical interpretation it is worth mentioning the geometrical interpretation of $(A_0 - A_1)/2$. This frequency is related to the phase, $(A_0 - A_1)/2eB$, acquired along one period of the open trajectory in Fig. 3. That the oscillations in Eqn. 43 appear to linear order in c relates to the fact that this trajectory contains a single reflection from magnetic breakdown junction.

VIII. CONCLUSIONS

Standard magnetic quantum oscillations are explained by Bohr-Sommerfeld quantization of electron dynamics along closed electron trajectories in a magnetic field. The oscillations are periodic in inverse magnetic field and, according to Onsager, the frequency of the oscillations is equal to the area of the closed electron trajectory. We refer to this single-particle effect as “Onsager oscillations”. For an electron in a periodic potential (crystal lattice or artificial superlattice) there are multiple closed trajectories and hence there are multiple Onsager frequencies. Oscillations with frequencies which do not correspond to any closed electron trajectory have also been observed and have remained not fully understood for decades. We call these oscillations “non-Onsager oscillations”. We show that there are two mechanisms responsible for these oscillations: (i) single particle kinetics, and (ii) multi-electron correlations. Both mechanisms contribute to the Shubnikov-de Haas effect and only the second mechanism contributes to the de Haas-Van Alphen effect. Very recently, half-frequency non-Onsager quantum magnetic oscillations were discovered in measurements with a two dimensional electron gas in GaAs on a superlattice. We show that the half-frequency oscillations also have two mechanisms: (i) single particle kinetics, and (ii) single particle dynamics with account of impurities. Again, both mechanisms contribute to the Shubnikov-de Haas effect and only the second mechanism contributes to the De Haas-Van Alphen effect.

We have developed a comprehensive theory of non-Onsager quantum magnetic oscillations in the magnetic breakdown regime. Non-Onsager means that the frequency of these oscillation is equal to the area of a trajectory that an electron cannot transverse. Hence, they are not directly related to the Onsager quantization. Experimentally integer non-Onsager oscillations have been known for quite some time. Very recently half-frequency non-Onsager oscillations have also been observed.

We demonstrate that there are two mechanisms for the integer oscillations, (i) single particle kinetics, (ii) multi-electron correlations due to the Coulomb electron-electron interaction. The both mechanisms contribute to the Shubnikov-de Haas effect (transport) and only the second mechanism contributes to the De Haas-Van Alphen effect (equilibrium). We calculate the temperature dependence of quantum non-Onsager oscillations and hence explain why they survive up to relatively high temperatures in spite of being fully quantum.

There are also two mechanisms for the half integer oscillations, both mechanisms are single particle (i) single particle kinetics, (ii) single particle dynamics with account of impurities. The both mechanisms contribute to the Shubnikov-de Haas effect (transport) and only the second mechanism contributes to the De Haas-Van Alphen effect (equilibrium).

To summarise, we explain the newly discovered half-frequency non-Onsager quantum magnetic oscillations and resolve the long standing theoretical controversy of integer non-Onsager quantum magnetic oscillations.

ACKNOWLEDGMENTS

This work was funded by the Australian Research Council Centre of Excellence in Future Low-Energy Electronics Technology (FLEET) (Grant No. CE170100039).

Appendix A: Theory of the scattering phase in magnetic breakdown

To compute the scattering phase we first map the scattering problem to the Landau-Zener problem (Ref. [32]) and then make use of Zener’s result [32] to obtain the scattering phase.

Semi-classical orbits exist in mechanical momentum space, defined by $[k_x, k_y] = ieB$. This is the space in which the circular orbit of Fig. 1 lives. At the intersection between two orbits we have two bands coupled by an off-diagonal matrix element W . The Hamiltonian is

$$H = \begin{bmatrix} ((k_x - g)^2 + k_y^2)/2m & W \\ W & (k_x^2 + k_y^2)/2m \end{bmatrix}$$

We then linearise this Hamiltonian around the intersection point $\mathbf{k}_0 = (g/2, \sqrt{k_F^2 - g^2}/4)$ (see Fig. 3a) and impose an on-shell condition, $H\psi = \varepsilon_F\psi$. If we define $\mathbf{k} = \mathbf{k}_0 + (eBX, P)$ then X and P give the deviation from the intersection point and are canonically conjugate. When the condition $H\psi = \varepsilon_F\psi$ is made linear in the variables X and P we obtain

$$-i\partial_X\psi = \begin{bmatrix} +\frac{eBk_{x0}}{k_{y0}}X & -\frac{mW}{k_{y0}} \\ -\frac{mW}{k_{y0}} & -\frac{eBk_{x0}}{k_{y0}}X \end{bmatrix}\psi = \mathcal{H}\psi \quad (\text{A1})$$

Which follows from $P = -i\partial_X$. The above, effective Hamiltonian, \mathcal{H} has the same form as the Hamiltonian used by Zener in Ref. [32]. Re-writing Eqn. A1 in Zener's notation gives

$$\mathcal{H} = \begin{bmatrix} +\frac{\alpha}{2}t & f \\ f & -\frac{\alpha}{2}t \end{bmatrix}$$

In this notation $t = X$, $\alpha > 0$ and $f < 0$. The effective Schrödinger equation $\mathcal{H}\psi = -i\partial_t\psi$ has solutions that we write in the form

$$\psi = \begin{bmatrix} C_1(t)e^{+i\alpha t^2/4} \\ C_3(t)e^{-i\alpha t^2/4} \end{bmatrix}$$

Here, the component C_1 corresponds to the wave 1 in Fig. 3 and the component C_3 corresponds to the wave 3 in the same figure. Both waves are propagating towards the intersection point. Suppose that the particle is initially in the state 3 of Fig. 3a.

$$\begin{aligned} C_1(-\infty) &= 0 \\ |C_3(-\infty)| &= 1 \end{aligned}$$

The scattering phase is determined by the components at time $t = \infty$: $C_1(\infty)$ (which relates to transitions $3 \rightarrow 4$), $C_3(\infty)$ (which relates to transitions $3 \rightarrow 2$). The full details of the calculation are contained in Ref. [32], which describes how to reduce the effective Schrödinger equation to the Weber equation [33]. In the end the asymptotic wavevector amplitudes are determined by the parabolic cylinder functions (Eqns. 9.246 in Ref. [34]). The amplitudes are summarised in table I.

In table I we have $n = if^2/\alpha$. Since n is pure imaginary most of the factors in the these expressions have

unit magnitude. Consistent with our boundary conditions we have $|C_1(-\infty)| = 0$ and $|C_3(-\infty)| = 1$. And consistent with our expectations we have $|C_1(\infty)| = c$, and $|C_3(\infty)| = s$, where s is the probability of magnetic breakdown $s = \exp(-2\pi f^2/\alpha)$ (equivalent to Eqn. 3). In addition to information about the probability of magnetic breakdown, table I also contains information about the phase acquired during a quantum jump. For the transitions defined in Fig. 3a we have

$$\begin{aligned} 3 \rightarrow 2 &\implies \Delta\phi = 0 \\ 3 \rightarrow 4 &\implies \Delta\phi = \phi_R \end{aligned}$$

Where ϕ_R is the phase acquired upon reflection from a magnetic breakdown junction and is given by

$$\phi_R = +\frac{\pi}{4} - \arg\left(\Gamma\left(1 + i\frac{f^2}{\alpha}\right)\right) + 2\frac{f^2}{\alpha} \ln(\sqrt{\alpha}|t|) \quad (\text{A2})$$

Here Γ is the gamma function, and the variables f and α are defined by

$$f = \frac{mW}{k_F\sqrt{1 - (\frac{g}{2k_F})^2}} \quad \alpha = \frac{eBg}{k_F\sqrt{1 - (\frac{g}{2k_F})^2}}$$

The phase ϕ_R contains terms which are of the form A/eB ; that is, terms which simply give a correction to the areas of the Fermi surface. The true scattering phase should not contain these area corrections and should equal zero in the adiabatic limit (large W or $f^2/\alpha \rightarrow \infty$). The expression satisfying these conditions is

$$\varphi = +\frac{\pi}{4} - \arg\left(\Gamma\left(1 + i\frac{f^2}{\alpha}\right)\right) + \frac{f^2}{\alpha} \left(\ln\left(\frac{f^2}{\alpha}\right) - 1\right) \quad (\text{A3})$$

-
- [1] A. Abrikosov, *Fundamentals of the Theory of Metals* (Dover Publications, 2017).
 - [2] M. G. Priestley, L. M. Falicov, and G. Weisz, Experimental and Theoretical Study of Magnetic Breakdown in Magnesium, *Physical Review* **131**, 617 (1963), publisher: American Physical Society.
 - [3] A. Alexandradinata and L. Glazman, Geometric Phase and Orbital Moment in Quantization Rules for Magnetic Breakdown, *Physical Review Letters* **119**, 256601 (2017), publisher: American Physical Society.
 - [4] A. Alexandradinata and L. Glazman, Fermiology of Topological Metals, *Annual Review of Condensed Matter Physics* **14**, 261 (2023), eprint: <https://doi.org/10.1146/annurev-conmatphys-040721-021331>.
 - [5] S. Kunisada, S. Isono, Y. Kohama, S. Sakai, C. Bareille, S. Sakuragi, R. Noguchi, K. Kurokawa, K. Kuroda, Y. Ishida, S. Adachi, R. Sekine, T. K. Kim, C. Cacho, S. Shin, T. Tohyama, K. Tokiwa, and T. Kondo, Observation of small fermi pockets protected by clean CuO2 sheets of a high-Tc superconductor, *Science* **369**, 833 (2020), <https://www.science.org/doi/pdf/10.1126/science.aay7311>.
 - [6] K. Kurokawa, S. Isono, Y. Kohama, S. Kunisada, S. Sakai, R. Sekine, M. Okubo, M. D. Watson, T. K. Kim, C. Cacho, S. Shin, T. Tohyama, K. Tokiwa, and T. Kondo, Unveiling phase diagram of the lightly doped high-Tc cuprate superconductors with disorder removed, *Nature Communications* **14**, 4064 (2023), number: 1 Publisher: Nature Publishing Group.
 - [7] F. K. de Vries, S. Slizovskiy, P. Tomić, R. K. Kumar, A. Garcia-Ruiz, G. Zheng, E. Portolés, L. A. Ponomarenko, A. K. Geim, K. Watanabe, T. Taniguchi, V. Fal'ko, K. Ensslin, T. Ihn, and P. Rickhaus, Kagome

- quantum oscillations in graphene superlattices (2023).
- [8] D. Q. Wang, Z. Krix, O. P. Sushkov, I. Farrer, D. A. Ritchie, A. R. Hamilton, and O. Klochan, Formation of Artificial Fermi Surfaces with a Triangular Superlattice on a Conventional Two-Dimensional Electron Gas, *Nano Letters* 10.1021/acs.nanolett.2c04358 (2023), publisher: American Chemical Society.
 - [9] L. Onsager, Interpretation of the de Haas-van Alphen effect, *The London, Edinburgh, and Dublin Philosophical Magazine and Journal of Science* **43**, 1006 (1952).
 - [10] D. Q. Wang, D. Reuter, A. D. Wieck, A. R. Hamilton, and O. Klochan, Two-dimensional lateral surface superlattices in GaAs heterostructures with independent control of carrier density and modulation potential, *Applied Physics Letters* **117**, 032102 (2020).
 - [11] R. W. Stark and C. B. Friedberg, Interfering electron quantum states in ultrapure magnesium, *Journal of Low Temperature Physics* **14**, 111 (1974).
 - [12] D. Morrison and R. W. Stark, Two-lifetime model calculations of the quantum interference dominated transverse magnetoresistance of magnesium, *Journal of Low Temperature Physics* **45**, 531 (1981).
 - [13] R. R. Gerhardt, D. Weiss, and K. v. Klitzing, Novel magnetoresistance oscillations in a periodically modulated two-dimensional electron gas, *Physical Review Letters* **62**, 1173 (1989).
 - [14] R. A. Deutschmann, W. Wegscheider, M. Rother, M. Bichler, G. Abstreiter, C. Albrecht, and J. H. Smet, Quantum Interference in Artificial Band Structures, *Physical Review Letters* **86**, 1857 (2001), publisher: American Physical Society.
 - [15] F. A. Meyer, E. Steep, W. Biberacher, P. Christ, A. Lerf, A. G. M. Jansen, W. Joss, P. Wyder, and K. Andres, High-Field de Haas-Van Alphen Studies of κ -(BEDT-TTF) $_2$ Cu(NCS) $_2$, *Europhysics Letters* **32**, 681 (1995).
 - [16] A. Audouard, J.-Y. Fortin, D. Vignolles, R. B. Lyubovskii, L. Drigo, F. Duc, G. V. Shilov, G. Ballon, E. I. Zhilyaeva, R. N. Lyubovskaya, and E. Canadell, Quantum oscillations in the linear chain of coupled orbits: The organic metal with two cation layers θ -(ET) $_4$ CoBr $_4$ (C $_6$ H $_4$ Cl $_2$), *EPL (Europhysics Letters)* **97**, 57003 (2012), publisher: IOP Publishing.
 - [17] C. W. J. Beenakker, Guiding-center-drift resonance in a periodically modulated two-dimensional electron gas, *Physical Review Letters* **62**, 2020 (1989), publisher: American Physical Society.
 - [18] R. W. Winkler, J. P. Kotthaus, and K. Ploog, Landau band conductivity in a two-dimensional electron system modulated by an artificial one-dimensional superlattice potential, *Physical Review Letters* **62**, 1177 (1989), publisher: American Physical Society.
 - [19] A. D. Mirlin and P. Wölfle, Weiss oscillations in the presence of small-angle impurity scattering, *Physical Review B* **58**, 12986 (1998), publisher: American Physical Society.
 - [20] M. I. Kaganov and A. A. Slutskin, Coherent magnetic breakdown, *Physics Reports* **98**, 189 (1983).
 - [21] J. W. Eddy and R. W. Stark, de Haas—van Alphen Study of Coherent Magnetic Breakdown in Magnesium, *Physical Review Letters* **48**, 275 (1982), publisher: American Physical Society.
 - [22] J.-Y. Fortin and T. Ziman, Frequency Mixing of Magnetic Oscillations: Beyond Falicov-Stachowiak Theory, *Physical Review Letters* **80**, 3117 (1998), publisher: American Physical Society.
 - [23] V. M. Gvozdkov, Y. V. Pershin, E. Steep, A. G. M. Jansen, and P. Wyder, de Haas—van Alphen oscillations in the quasi-two-dimensional organic conductor κ -(ET) $_2$ Cu(NCS) $_2$: The magnetic breakdown approach, *Physical Review B* **65**, 165102 (2002), publisher: American Physical Society.
 - [24] B. L. Al'tshuler, A. G. Aronov, and B. Z. Spivak, The Aaronov-Bohm effect in disordered conductors, *JETP Letters* **33**, 101 (1981).
 - [25] A. B. Pippard, Quantization of coupled orbits in metals, *Proceedings of the Royal Society of London. Series A. Mathematical and Physical Sciences* **270**, 1 (1962), publisher: Royal Society.
 - [26] C. W. Groth, M. Wimmer, A. R. Akhmerov, and X. Waintal, Kwant: a software package for quantum transport, *New J. Phys.* **16**, 063065 (2014).
 - [27] M. Büttiker, Four-terminal phase-coherent conductance, *Phys. Rev. Lett.* **57**, 1761 (1986).
 - [28] O. A. Tkachenko, V. A. Tkachenko, D. G. Baksheev, and O. P. Sushkov, Wannier diagrams for semiconductor artificial graphene, *JETP Letters* **116**, 638 (2022).
 - [29] O. A. Tkachenko, V. A. Tkachenko, D. G. Baksheev, and O. P. Sushkov, Effect of disorder on magnetotransport in semiconductor artificial graphene, *JETP Letters* **117**, 222 (2023).
 - [30] I. M. Lifshits and A. M. Kosevich, Theory of Magnetic Susceptibility in Metals at Low Temperature, *Journal of Experimental and Theoretical Physics* **2**, 636 (1956).
 - [31] L. D. Landau and E. M. Lifshitz, CHAPTER VII - NON-IDEAL GASES, in *Statistical Physics (Third Edition)*, edited by L. D. Landau and E. M. Lifshitz (Butterworth-Heinemann, Oxford, 1980) pp. 225–250.
 - [32] C. Zener and R. H. Fowler, Non-adiabatic crossing of energy levels, *Proceedings of the Royal Society of London. Series A, Containing Papers of a Mathematical and Physical Character* **137**, 696 (1932), publisher: Royal Society.
 - [33] E. T. Whittaker and G. N. Watson, The Confluent Hypergeometric Function, in *A Course of Modern Analysis*, Cambridge Mathematical Library (Cambridge University Press, Cambridge, 1996) 4th ed., pp. 337–354.
 - [34] I. S. Gradshteyn and I. M. Ryzhik, 9 - Special Functions, in *Table of Integrals, Series, and Products (Eighth Edition)*, edited by D. Zwillinger and V. Moll (Academic Press, Boston, 2014) pp. 1014–1059.

C	$t \rightarrow -\infty$	$t \rightarrow +\infty$
C_1	$\alpha^{-\frac{n}{2}} t ^{-n} e^{-i\frac{\pi}{4}} e^{-i\alpha t^2/2} \frac{f}{\alpha t }$	$e^{-i \arg(\Gamma(n+1))} \alpha^{\frac{n}{2}} t ^n (1-P)^{1/2}$
C_3	$\alpha^{-\frac{n}{2}} t ^{-n} e^{-i\frac{\pi}{4}}$	$\alpha^{-\frac{n}{2}} t ^{-n} e^{-i\frac{\pi}{4}} P^{1/2}$

Table I. Summary of the asymptotic components of the wavevector ψ .